

Comparative Study of Dark Matter Relic Density in IDM, MSSM and NMSSM

Mohid Farhan*

Department of Space Science, Institute of Space Technology, Islamabad, Pakistan

(Dated: December 11, 2025)

This article presents a computational comparison of relic density predictions for three prominent frameworks Beyond the Standard Model (BSM): the Inert Doublet Model (IDM), the Minimal SuperSymmetric Standard Model (MSSM), and the Next-to-Minimal SuperSymmetric Standard Model (NMSSM). Using MicrOMEGAs, we calculate relic densities over varying mass ranges in the low coupling regime. We highlight key differences in each model's behavior relative to current observational bounds and identify viable mass regions. The findings contribute towards guiding model selection based on relic density constraints and suitability.

I. INTRODUCTION

In 1931, Fritz Zwicky noticed that objects residing away from the center of their respective galaxies, travel faster than the predictions of Newtonian mechanics [1]. After a few decades, it was confirmed by the discovery of Galactic Rotation Curves [2, 3]. This suggested the existence of non-luminous matter, therefore being labeled "dark matter". There exist many models beyond the Standard Model (BSM), that attempt to explain this anomaly by introducing new particles beyond the Standard Model, e.g the Inert Doublet Model (IDM) [5], Minimal Super-Symmetric Model (MSSM) [7] and Next to Minimal Super-Symmetric Model (NMSSM) [8]. Although several other extensions of the Standard Model exist, this study provides a comparison restricted to just these models. The aim is to provide a cross-model analysis of the responses to different dark matter masses in the light and heavy regions and capture the sensitivity of the dark matter relic density to subtle variations in parameter space. By incorporating relic density observational bounds[17], viable dark matter mass regions are also determined for each model in their respective parameter space. These viable regions must also satisfy indirect constraints from gamma-ray observations of dwarf spheroidal galaxies [14]. Although these models have been extensively studied individually and MSSM-NMSSM comparisons are readily available in literature [11], there are limited cross-model comparisons that also include doublet extension models, like the IDM, which can depict the contrast in experimental results for different kinds of models and be useful as a reference for new physics model selections.

II. THEORETICAL FRAMEWORK

Inert Doublet Model (IDM)

IDM is a doublet extension to the standard model (SM), as it hypothesizes an inert doublet, where the lightest scalar (H_1) is the dark matter candidate [4, 5].

"Inert" implies that the doublet does not gain a Vacuum Expectation Value (VEV), and is therefore, unable to participate in Electro-Weak Symmetry Breaking (EWSB). The doublets are represented by:

$$\phi_1 = \begin{pmatrix} G^+ \\ \frac{v+h+iG^0}{\sqrt{2}} \end{pmatrix}, \phi_2 = \begin{pmatrix} H_1^+ \\ \frac{H_1^0+iA_1^0}{\sqrt{2}} \end{pmatrix} \quad (1)$$

Each doublet contains a charged and neutral component. ϕ_1 is the active Higgs doublet in the SM, as indicated by the nonzero vacuum expectation value v , which is responsible for electroweak symmetry breaking via the Higgs mechanism. It is through this mechanism that the Standard Model particles acquire mass. The physical Higgs boson is represented by h , with an experimentally measured mass of about 125 GeV. The fields G^+ and G^0 are the Goldstone bosons. On the other hand, a Z_2 symmetry is imposed on ϕ_2 to make the dark matter candidate stable and inert, where the inert doublet is odd under Z_2 transformations:

$$\phi \rightarrow -\phi$$

and the SM particles are even under Z_2 transformations:

$$\phi \rightarrow \phi$$

H_1^0 is the dark matter candidate (CP-even scalar) and A_1^0 is the CP-odd scalar. The Lagrangian of IDM is the sum of the Standard Model Lagrangian terms and terms involving an additional scalar doublet ϕ_2 that is odd under a Z_2 symmetry:

$$\mathcal{L}_{\text{IDM}} = \mathcal{L}_{\text{SM}} + (D_\mu \phi_2)^\dagger (D^\mu \phi_2) - V(\phi_1, \phi_2) \quad (2)$$

The scalar potential is:

$$V(\phi_1, \phi_2) = \mu_1^2 |\phi_1|^2 + \mu_2^2 |\phi_2|^2 + \lambda_1 |\phi_1|^4 + \lambda_2 |\phi_2|^4 \quad (3)$$

$$+ \lambda_3 |\phi_1|^2 |\phi_2|^2 + \lambda_4 |\phi_1^\dagger \phi_2|^2 + \left[\frac{\lambda_5}{2} (\phi_1^\dagger \phi_2)^2 + \text{h.c.} \right] \quad (4)$$

The coupling constant relevant to us is λ_L which is given by:

$$\lambda_L = \frac{1}{2} (\lambda_3 + \lambda_4 + \lambda_5) \quad (5)$$

* mohidf35@gmail.com

which depicts the interaction of the Dark Matter (DM) candidate with the Higgs boson. The IDM parameter space is severely constrained by vacuum stability, perturbativity, and most recently, the measured properties of the 125 GeV Higgs boson at the LHC [6]. The mass-deficit between the CP-even and odd candidates within the inert doublet is given by δ . Relic density dependence on λ_L with varying DM mass (m_{DM}) and δ is discussed later.

Minimal Super-Symmetric Standard Model (MSSM)

The Minimal Super-Symmetric model postulates that every fermionic SM particle has a supersymmetric (SUSY), bosonic counterpart and vice versa. The SUSY particles can be distinguished from SM particles by R-parity operator, which is depicted by:

$$\hat{R} = (-1)^{3(B-L)+2s} \quad (6)$$

where B and L are Baryon and Lepton numbers and s shows the spin state. All SM and SUSY particle return eigenvalues of 1 and -1, respectively under the R-parity operator. This conservation ensures the stability of the Lightest SUSY particle (LSP) or neutralino ($\tilde{\chi}_1^0$), which is the dark matter candidate. Unlike IDM, the mass of the dark matter candidate is a derived quantity that is computed by diagonalizing the mass matrix [7]. The neutralino mass matrix in the MSSM, expressed in the basis $(\tilde{B}, \tilde{W}^0, \tilde{H}_d^0, \tilde{H}_u^0)$, determines the composition of the LSP and its interactions. The full expression is well-established [7]. The Bino (\tilde{B}), Wino (\tilde{W}^0) and Higgsinos ($\tilde{H}_d^0, \tilde{H}_u^0$) mixings ultimately determine the mass and properties of dark matter candidate.

$$\tilde{\chi}_1^0 = N_{11}\tilde{B} + N_{12}\tilde{W}^0 + N_{13}\tilde{H}_d^0 + N_{14}\tilde{H}_u^0 \quad (7)$$

The crucial parameters are M_1 (Bino mass), M_2 (Wino mass), μ (Higgsino mixing) and $\tan\beta$, which is the ratio of VEVs for the up-type to the down-type Higgs doublets. μ appears in the superpotential:

$$W_{MSSM} = W_{Yukawa} + \mu H_u H_d \quad (8)$$

The effects of μ and $\tan\beta$ on relic density will be shown in the results and discussion section. μ comes with a naturalness issue since its mass is not constrained by any symmetry, which means that it can be as large as the Planck Mass and so naturalness becomes a problem.

Next-to-Minimal Supersymmetric Standard Model (NMSSM)

The NMSSM is a singlet extension of the MSSM, naturally solves the ' μ problem'. A gauge singlet superfield \hat{S} is introduced in addition to the two Higgs doublets. This introduces new terms to the superpotential:

$$W_{NMSSM} = W_{Yukawa} + \lambda \hat{S} \hat{H}_u + \frac{1}{3} \kappa \hat{S}^3 \quad (9)$$

The mass matrix is now a basis of $(\tilde{B}, \tilde{W}^0, \tilde{H}_d^0, \tilde{H}_u^0, \hat{S})$ [8, 10] This removes μ from the superpotential, which naturally solves the μ problem, while introducing a richer Higgs and neutralino spectrum. It also opens up new annihilation channels and offers more flexibility. In the SUSY models, the lightest supersymmetric particle (LSP) is often considered the dark matter candidate since R-parity forces it to remain inert. While solving the μ -problem, the NMSSM introduces new constraints from searches for light Higgs bosons and exotic decays at the LHC [12].

III. METHODOLOGY

The relic density Ωh^2 of the dark matter candidate is computed using micrOMEGAs, a numerical package designed to evaluate dark matter observables across BSM frameworks. For each model, the particle content and interactions are specified via model files in CalcHEP format [18, 19]. The time evolution of the dark matter number density n_χ is governed by the Boltzmann equation, which micrOMEGAs solves numerically:

$$\frac{dn_\chi}{dt} + 3Hn_\chi = -\langle\sigma v\rangle (n_\chi^2 - n_\chi^{\text{eq}2}), \quad (10)$$

where H is the Hubble parameter, $\langle\sigma v\rangle$ is the thermally averaged annihilation cross-section, and n_χ^{eq} is the equilibrium number density. MicrOMEGAs computes the thermally averaged cross-section using:

$$\langle\sigma v\rangle = \frac{1}{8m_\chi^4 T K_2^2(m_\chi/T)} \int_{4m_\chi^2}^{\infty} ds \sigma(s) (s - 4m_\chi^2) \sqrt{s} K_1(\sqrt{s}/T), \quad (11)$$

where K_1 and K_2 are modified Bessel functions, and $\sigma(s)$ includes all $2 \rightarrow 2$ annihilation and coannihilation channels. The relic abundance is derived via numerical integration over temperature:

$$\Omega_\chi h^2 = \frac{1.07 \times 10^9 \text{ GeV}^{-1}}{g_*^{1/2} M_{\text{Pl}} \int_{x_f}^{\infty} \frac{\langle\sigma v\rangle}{x^2} dx}, \quad (12)$$

where $x = m_\chi/T$, x_f is the freeze-out point, g_* denotes effective relativistic degrees of freedom, and M_{Pl} is the Planck mass. The relic density of dark matter is constrained to be in the region:

$$\Omega h^2 = 0.1199 \pm 0.0027 \quad (13)$$

by Planck data [17]. To maintain consistency with observation, we will include these bounds in our computational analysis.

IV. RESULTS AND DISCUSSION

In this section, we present the dark matter relic density as a function of key parameters for the models, including a cross-model comparison using dark matter

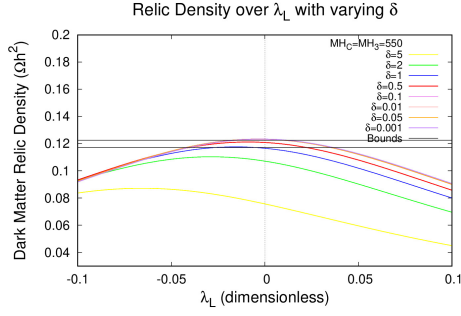


FIG. 1. Dark matter relic density as a function of DM-Higgs coupling for varying δ .

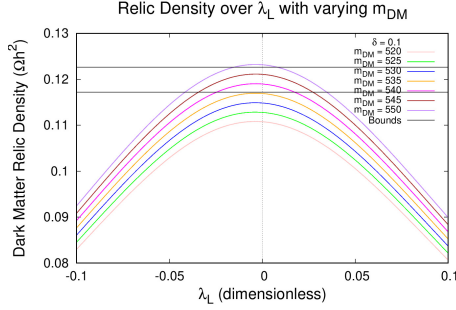


FIG. 2. Dark matter relic density as a function of DM-Higgs coupling λ_L for varying δ in IDM.

mass. Figure 1 is plotted for $m_{DM} \approx 550$ GeV in IDM. As δ approaches zero, inverting the sign of λ_L yields the same relic density values due to the dominance of the $H_1 A_1$ annihilation, for which the cross section scales as λ_L^2 . This apparent symmetry along $\lambda_L = 0$ is lost as δ increases and the population of A_1 drops due to Boltzmann suppression [5] and other annihilation channels with linear dependencies on λ_L start contributing to the relic density. It is also shown that greater values of δ leads to better annihilation due to the effectiveness of the $H_1 H_1 \rightarrow f \bar{f}$ channel that gains relevance as δ deviates from 0 as shown in Figure 1.

Figure 2 verifies that relic density is highest at low λ_L , which is obvious since low couplings lead to overabundance. It also demonstrates that for the region $350 \text{ GeV} < m_{DM} < 650 \text{ GeV}$, an increase in dark matter mass corresponds to an increase in relic density at $\delta = 0.1$. Therefore in this parameter space, increasing the mass of dark matter leads to a higher relic density. Under the Planck bounds [17], the viable dark matter mass window is $536 \text{ GeV} \leq m_{DM} \leq 548 \text{ GeV}$.

As for MSSM, Figure 3 illustrates the behavior of relic density as $\tan \beta$ and μ are varied. We observe resonance peaks in the $\mu \leq 100$ region followed by a plateau in the relic density as the LSP transitions to Higgsino-like to Bino-like. At low $\tan \beta$, the Higgs coupling to down-type quarks are weak, which suppresses s-channel processes and leads to a broad relic density peak. As we increase $\tan \beta$, the Yukawa couplings are enhanced

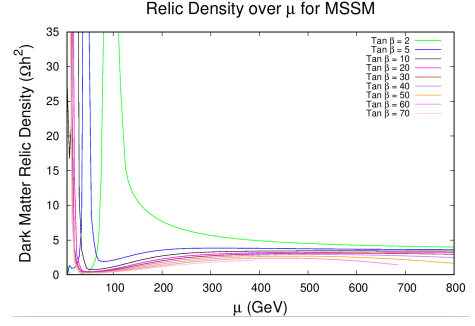


FIG. 3. Relic density in MSSM as a function of μ and $\tan \beta$, showing resonance peaks and the effect of LSP composition.

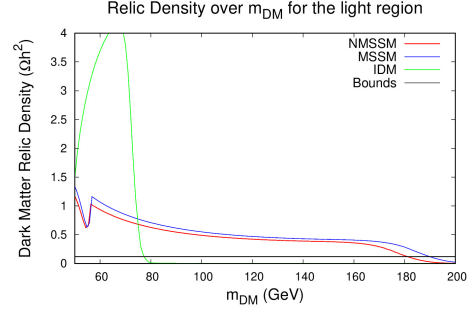


FIG. 4. Cross-model comparison of IDM, MSSM, and NMSSM relic densities in the light dark matter mass regime.

which leads to efficient annihilation, narrower peaks and lower relic density. The narrowing occurs because a smaller Higgsino admixture is sufficient to trigger effective annihilation at high, while the earlier onset reflects stronger coupling to Higgs bosons. This behavior highlights the sensitivity of neutralino relic density to both the LSP composition and the Higgs-fermion coupling hierarchy driven by $\tan \beta$. Moreover, the discontinuity in peaks at high $\tan \beta$, and μ , depicts the breakdown of mass generation spectrum as a result of unphysical and results like imaginary masses, showcasing the importance of $\tan \beta$ on the validity of the model. In QFT, "imaginary mass" implies a tachyonic instability or a wrong vacuum.

The only truly comparable parameters, across all 3 models, are mass of the dark matter candidate and relic density. This motivates us to draw a comparison, however, since the mass is a derived quantity in SUSY models, it could not be directly defined. To ensure a systematic increase in dark matter mass, M_2 and μ were made large at 2000 and 1500 GeV respectively, and M_1 was increased. The decoupling of the Higgsinos and Wino meant that $m_{DM} \approx M_1$. In the light region, the mass of the sleptons was capped at 400 GeV, and a light mass region $50 \text{ GeV} < m_{DM} < 200 \text{ GeV}$ was studied in figure 4.

This revealed the Higgs resonance drop in IDM at around $m_{DM} \approx M_h/2$, where $M_h = 125 \text{ GeV}$, is the mass of the Higgs boson. The mass-splitting between

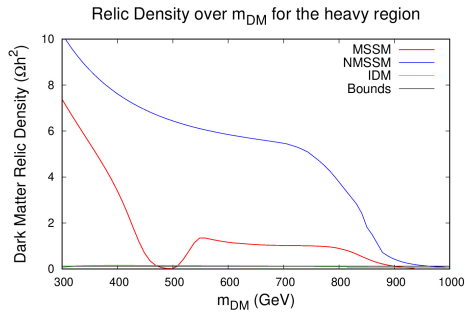


FIG. 5. Cross-model comparison of IDM, MSSM, and NMSSM relic densities in the heavy dark matter mass regime.

the dark matter candidate and its charged and CP-odd counterparts were kept large to mimic a lack of fine tuning. The resulting light region viable mass is $m_{IDM} \approx 78$ GeV. On the contrary, the SUSY models show a gradual decrease in relic density as mass increases, since the neutralino becomes less Bino-like. The sleptons (Supersymmetric counterparts of the Leptons) needs to be at least 100-120 GeV heavier than the Bino mass to ensure that the LSP does not become electrically charged, which is an invalid result for dark matter. M_1 and μ are kept around 1 TeV each. The Higgs resonance dip for SUSY models is not as prominent as in IDM. λ is kept small ($\lambda \approx 0.05$) to allow for mass spectrum generation without unphysical and imaginary masses, which results in the SUSY relic densities remain close to each other. Bino is notorious for overproducing dark matter due to inefficient annihilation. Wino and Higgsinos, on the other hand, annihilate too effectively and lead to underabundance of dark matter. This explains the gradual decrease in relic density since, as we increase bino mass, the LSP becomes less Bino-like and even a small fraction of Higgsino interaction leads to a decrease in relic density. The MSSM gives observable relic density values in the light region at $m_{MSSM} \approx 190$ GeV whereas the NMSSM does so at $m_{NMSSM} \approx 181$ GeV. To address the naturally predicted DM overabundance, the relic density is often brought down by co-annihilation channels (e.g., bino-wino or stop co-annihilation) or resonant annihilations [9]. Although recent experimental constraints strongly disfavor large portions of the 50–200 GeV mass window, our results identify narrow viable regions across all three models, particularly near resonance channels, where the relic density falls within or below the Planck bound. These regions remain phenomenologically relevant, provided they also evade direct and indirect detection limits [15, 16], which is for a future study.

Then in Figure 5, we transition to the heavy region, where μ and M_2 are increased to 1.5 and 2 TeV respectively, to increase the window of a Bino-dominant LSP. The sLepton masses were also increased to 1 TeV to avoid a charged LSP, as mentioned earlier. These modifications allowed us to obtain results for a heavy LSP mass region of $300 \text{ GeV} < m_{DM} < 1000 \text{ GeV}$. The SUSY

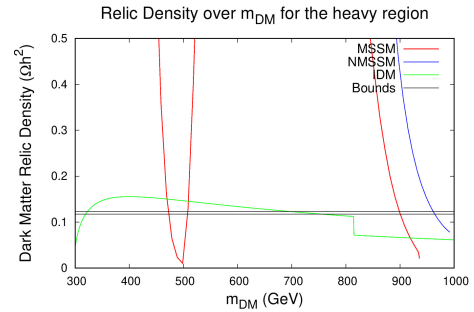


FIG. 6. Zoomed-in view of IDM, MSSM, and NMSSM relic densities at heavy dark matter masses, highlighting viable regions consistent with observational constraints.

models continued their decreasing trend whereas the IDM remained relatively close to experimental Higgs bounds. The most notable difference was in the resonance dip at around 500 GeV for MSSM, and the subsequent difference in relic density from NMSSM. This stems from the case that $2m_{DM} \approx m_l$, which breaks open the annihilation channel:

$$\tilde{\chi}_1^0 \tilde{\chi}_1^0 \rightarrow l^+ l^- \quad \text{via } \tilde{l} \text{ (t-channel)}$$

The effectiveness of this channel is apparent in the MSSM, but its effects are damped by the singlino component of the LSP in the NMSSM, despite small coupling. The new CP-even and CP-odd scalars introduce s-channel interactions, which dilute the effects of the t-channel interactions, as the probability of t-channel interactions decrease at the expense of an increase in probability of s-channel interactions. Since the s-channel interactions are not efficient, the relic density stays relatively high in the NMSSM.

Figure 6 zooms in on the Higgs bounds for viable DM mass analysis. The IDM follows the Higgs bounds closely and gives the widest region of dark matter relic density mass, with minimal fine-tuning, at $700 < m_{IDM} < 755$ GeV. The l-channel dip for the MSSM yield 2 very narrow viable dark matter regions at $m_{MSSM} \approx 470$ GeV and $m_{MSSM} \approx 505$ GeV, and later naturally decreases to observable bounds by $m_{MSSM} \approx 900$ GeV. The only window of viability for NMSSM is shown to be $m_{NMSSM} \approx 960$ GeV. The abrupt drop and end of the MSSM and NMSSM curves is due to the breakdown of the approximately equal relation of the LSP mass to the Bino mass, since the mass of the Leptons becomes comparable to Bino mass as it approaches 1 TeV which plateaus the LSP mass.

V. CONCLUSION

This study presents a comparative relic density analysis of the IDM, the MSSM, and the NMSSM across both light and heavy dark matter mass regimes. By isolating relic density and dark matter mass as the

only directly comparable observables, their behavior has been mapped under unified scan conditions. Our results confirm well-known resonance effects near in all three models but reveal a distinctive slepton-induced annihilation dip in the MSSM near 500 GeV, absent in the NMSSM due to singlino dilution and competing annihilation channels. Despite stringent experimental constraints, particularly in the sub-200 GeV range, we identify narrow viable bands in all models that remain consistent with the Planck relic density bound. A direct comparison assists in selecting a new physics model

consistent with the reader’s requirements, depending on the region. Models like Z_3M , Z_4IDSM , Z_5M and Z_7M , along with other variations of the MSSM, like CMSSM, can be studied for a more versatile comparison. The comparison will aid in observing the effects of different symmetries and variations of singlet and doublets extensions on dark matter relic density. By quantifying fine-tuning, we can distinguish which models suffer from fine tuning from naturally feasible models, with particular attention to limits from LZ [15] and XENONnT [16], and PandaX [13].

-
- [1] F. Zwicky, *On the Masses of Nebulae and of Clusters of Nebulae*, Astrophysical Journal, **86**, 217–246 (1937).
 - [2] M. J. Disney and J. Silk, “Dark matter and the rotation curves of galaxies,” *Nature*, vol. 263, pp. 573–575, 1976.
 - [3] V. C. Rubin, N. Thonnard, and W. K. Ford, *Rotational Properties of 21 Sc Galaxies with High Luminosities. I. The Data*, Astrophys. J. **238**, 471–487 (1980).
 - [4] N.G. Deshpande and E. Ma, *Pattern of Symmetry Breaking with Two Higgs Doublets*, Phys. Rev. D, **18**, 2574 (1978).
 - [5] M. Gustafsson, “The inert doublet model and its phenomenology,” *arXiv preprint arXiv:1106.1719*, 2011.
 - [6] A. Goudelis, B. Herrmann, and O. Stål, *Dark matter in the inert doublet model after the discovery of a Higgs-like boson at the LHC*, J. High Energy Phys. **08**, 019 (2013).
 - [7] S. Dawson, “The MSSM and why it works,” *arXiv preprint hep-ph/9712464*, 1997.
 - [8] L. Meng, J. Cao, F. Li, and S. Yang, “Dark Matter Physics in General NMSSM,” *J. High Energy Phys.*, vol. 2024, no. 8, pp. 212, 2024.
 - [9] G.H. Duan *et al.*, *Probing bino-wino coannihilation dark matter under the neutrino floor at the LHC*, Phys. Rev. D **98**, 015010 (2018).
 - [10] U. Ellwanger, C. Hugonie, and A.M. Teixeira, *The Next-to-Minimal Supersymmetric Standard Model*, Phys. Rept., **496**, 1–77 (2010). arXiv:0910.1785.
 - [11] S. Porto, G. A. Moortgat-Pick, and K. Rolbiecki, “Towards discrimination of MSSM and NMSSM scenarios at colliders,” **International Workshop on Future Linear Colliders, LCWS13**, Tokio, Japan (2013) arXiv:1404.1053
 - [12] D. Das, U. Ellwanger, and A.M. Teixeira, *LHC constraints on $M_{1/2}$ and m_0 in the semi-constrained NMSSM*, J. High Energy Phys. **04**, 022 (2013).
 - [13] H. B. Cui *et al.* [PandaX-II Collaboration], *Dark Matter Results From First 98.7 Live Days of PandaX-II Experiment*, Phys. Rev. Lett. **117**, 121303 (2016).
 - [14] M. Ackermann *et al.* [Fermi-LAT Collaboration], *Searching for Dark Matter Annihilation from Milky Way Dwarf Spheroidal Galaxies with Six Years of Fermi-LAT Data*, Phys. Rev. Lett. **115**, 231301 (2015).
 - [15] J. Aalbers *et al.* [LZ Collaboration], *First Dark Matter Search Results from the LUX-ZEPLIN (LZ) Experiment*, Phys. Rev. Lett., **131**, 041002 (2023).
 - [16] E. Aprile *et al.* [XENON Collaboration], *Search for New Physics in Electronic Recoil Data from XENONnT*, Phys. Rev. Lett., **129**, 161805 (2022).
 - [17] N. Aghanim *et al.* [Planck Collaboration], “Planck 2018 results. VI. Cosmological parameters,” *Astronomy & Astrophysics*, vol. 641, A6, 2020. arXiv:1807.06209
 - [18] G. Bélanger, F. Boudjema, A. Pukhov and A. Semenov, “micrOMEGAs: A tool for dark matter studies,” *Comput. Phys. Commun.*, vol. 182, no. 4, pp. 842–856, Apr. 2011.
 - [19] G. Bélanger *et al.*, *micrOMEGAs5.0: Freeze-in*, Comput. Phys. Commun., **231**, 173–186 (2018).